Simulations of dune morphology under tri-directional wind regimes and application to dunes on Mars

David Rubin, Olivier Rozier, Clément Narteau, Sylvain Courrech Du Pont

Aeolian Research 67–69 (2024) 100922

Contents lists available at ScienceDirect

Aeolian Research

journal homepage: www.elsevier.com/locate/aeolia

Simulations of dune morphology under tri-directional wind regimes and application to dunes on Mars

David M. Rubin [a,*], Olivier Rozier [b], Clément Narteau [b], Sylvain Courrech du Pont [c]

[a] Department of Earth and Planetary Sciences, University of California Santa Cruz, 1156 High St., Santa Cruz, CA 95064, USA
[b] Institut de Physique du Globe de Paris, Université Paris Cité, CNRS, Paris, France
[c] Laboratoire Matière et Systèmes Complexes, Université Paris Cité, CNRS, Paris, France

ARTICLE INFO

Keywords:
Dunes
Ripples
Bedforms
Mars
Aeolian

ABSTRACT

Dune morphology was simulated using coupled models of wind flow and sand transport for 4728 tri-directional wind regimes and bed conditions. The dominant control of dune morphology is sand coverage on the bed. Dunes on a fully sand-covered bed tend to form a periodic pattern of long crests with a relatively uniform spacing. In contrast, dunes on a starved bed have greater diversity of crest orientations and shapes, including complex shapes that have not been simulated or observed in bidirectional wind regimes. These specific dune shapes resulting from the tri-directional wind regime persist regardless of whether the transport capacity of the weakest wind is comparable to or only 1/10th that of the dominant wind.

On sand-covered beds, dunes generally have only a single modal orientation (approximately that with maximum gross bedform-normal transport). The exceptions are where two strong winds diverge by 90° (two dune orientations arise), where three winds have triradial symmetry (three dune orientations), or winds have modest deviations from triradial symmetry (two dune orientations).

On a starved bed, increasing the divergence angle between two strong winds produces a highly generalized sequence of: barchan dunes (divergence angle ~30° between the two dominant winds), squat barchans or domes (divergence angle of ~60°), dunes with two or three crest orientations (divergence angles ~90° or 120°), to slug-shaped or boomerang-shaped dunes (divergence angle 180°, i.e., reversing winds). The simulated morphologies include a wide variety of Martian dune shapes, which allows their formative wind regimes to be inferred.

1. Introduction and previous work

1.1. Purpose

As part of NASA's Mars Data Analysis Program, we developed a new approach to use dune morphology to constrain interpretations of multi-directional wind regimes on Mars. Instead of trying to interpret each individual variety of dune using whatever is known about that observed morphology, we used the Pleiades supercomputer to simulate dune morphology for thousands of combinations of wind regimes and bed conditions. Simulated wind regimes had three directional modes with differing relative magnitudes; previous studies generally have been restricted to wind regimes with two directional modes. Bed conditions were fully sand-covered or partially starved. We then used the resulting simulated morphologies to constrain the formative wind regimes of representative dune morphologies on Mars.

1.2. Previous simulations

As early as the 1990s, researchers began developing models to relate dune morphology to bidirectional winds. The early simple models lacked detailed fluid interactions with the bed but were nevertheless able to recreate simple dunes and their behavior utilizing bulk transport of slabs of sand (Werner, 1995). Later models incorporated additional fluid/sediment processes and were able to create a broader range of morphologic details of dunes in bidirectional flows (Nishimori and Tanaka, 2003; Parteli et al., 2009; Parteli et al., 2014; and publications described in the Methods Section 2.)

1.3. Previous field and lab studies of dune morphology and orientation

Until the 1980s, models of dune morphology and orientation were based on qualitative measurements or small numbers of field

* Corresponding author.
E-mail address: drubin@ucsc.edu (D.M. Rubin).

https://doi.org/10.1016/j.aeolia.2024.100922
Received 22 August 2023; Received in revised form 11 February 2024; Accepted 16 March 2024
Available online 26 March 2024

observations. These studies led geomorphologists and sedimentologists to believe that ripples and dunes formed with orientations that were either transverse or parallel to the resultant sand-transport direction. The factor controlling a transport-parallel (longitudinal) orientation was thought to be bidirectional wind (Bagnold, 1941), although Bagnold did not quantify what conditions—angle between the two winds (divergence angle) and their relative strength (transport ratio)—were required to produce the two differing orientations.

Dunes with oblique orientations have also been recognized, but before the 1980s they were generally thought to be aberrations due to special circumstances, such as winds that rotated through time or space faster than dunes could adjust orientation, orientation of the sand source, along-crest differences in migration speed that caused dunes to rotate, dunes originating parallel to a sand supply, or other conditions listed by Rubin and Hunter (1987). Over the past few decades, many experimental and theoretical studies have investigated morphology of ripples and dunes in a broad range of bidirectional flows (Rubin and Hunter, 1987; Rubin and Ikeda, 1990; Werner and Kocurek, 1997; Parteli et al., 2009; Reffet et al., 2010; Courrech du Pont et al., 2014; Ping et al., 2014; Gao et al., 2015b; Lucas et al., 2015; Gadal et al., 2019; Rozier et al., 2019; Gadal et al., 2020), and these studies have shown that some bidirectional winds (obtuse divergence angle and transport ratio $\neq 1$) produce dunes that are oblique to the net sand-transport direction, even in the absence of external complications. In addition, these studies have shown that in areas of high sand availability, periodic dune patterns grow in height and migrate, adopting an orientation that is more perpendicular to the dominant wind than to the weaker wind. In contrast, dunes that elongate on a starved bed adopt an orientation that is somewhat more aligned with the dominant wind. This observation has led to the identification of two distinct dune growth mechanisms that explain, according to sand availability, the coexistence of dunes with different orientations under the same bidirectional wind regimes (Courrech du Pont et al., 2014; Lü et al., 2022).

Unidirectional winds blowing over a partially starved bed of non-cohesive sand form symmetrical barchan dunes (Bagnold, 1941), but many barchan dunes are laterally asymmetric. The asymmetry has been attributed to bimodal winds (Bagnold, 1941; Tsoar, 1984), to dune interactions, to spatially varying winds, topography, or sand supply (Bourke, 2010; Parteli et al., 2014). Bagnold's and Tsoar's conceptual models, in which asymmetry arises purely from a bimodal wind, predict opposite asymmetries. Lv et al. (2016) found that in some bimodal winds, the asymmetry matched Bagnold's predictions, whereas in other bimodal winds the morphology matched Tsoar's predictions (dependent on divergence angle and transport ratio). In all cases, the longer arm is more aligned with the dominant wind, demonstrating that it elongates away from the migrating dune body.

Although numerous studies have investigated dune morphology for a wide range of bimodal wind regimes, to our knowledge no previous studies have investigated dune morphology in trimodal winds. A few studies have found, however, that at least three winds are required to produce specific kinds of dunes such as star dunes (Zhang et al., 2012) or raked linear dunes (Lü et al., 2017). Introducing a third wind can cause two substantial changes in dune dynamics and morphology. First, a bimodal wind regime with zero net transport is restricted to the single case of two equal and opposite winds. In contrast, a third wind allows the possibility of many wind regimes with zero net transport. Second, in a bimodal wind regime only two orientations can have (equal) maximum gross bedform-normal transport (orthogonal dune orientations), whereas a regime with three winds can produce three such orientations.

Our simulations—which include the complexities of crest reversals and defect dynamics— demonstrate that multidirectional wind regimes can generate distinct varieties of bedforms, with different orientations resulting from the same growth mechanism (Zhang et al., 2012), or from different growth mechanisms (Lü et al., 2017). These morphologies can be interpreted using the theoretical framework provided by Courrech du Pont et al. (2014).

2. Methods

To simulate dune morphology, we used the cellular automaton model of Narteau et al. (2009) and Rozier and Narteau (2014). This model later proved well suited to investigate dune shapes in a variety of bed conditions and wind regimes (Zhang et al., 2012; Lucas et al., 2014; Gao et al., 2015b; Lü et al., 2017; Lü et al., 2018; Rozier et al., 2019; Gadal et al., 2020). The model reproduces most physical processes that relate to sand transport (erosion, deposition, and avalanches). Unlike other cellular automaton approaches, our sediment transport model is coupled with a fluid dynamics component, so that it fully accounts for feedback mechanisms between the wind flow and the topography (*e.g.*, shear stress at the bottom of the turbulent layer, air flow speed-up toward the dune crest).

As observed in nature (Ping et al., 2021), a flat sand bed, exposed to a unidirectional wind, destabilizes into periodic dunes with a characteristic wavelength, λ_0 (Claudin and Andreotti, 2006; Narteau et al., 2009). In nature, this characteristic wavelength, λ_0, depends on sediment and atmospheric properties and flow regime, and can be used to rescale and quantitatively compare the numerical simulations and the different natural environments where the dune instability is observed. On Earth, λ_0 is reported to be between 15 and 20 m (Elbelrhiti et al., 2005; Ping et al., 2021). On Mars, λ_0 is not accurately known; Durán Vinent et al. (2019) estimate a range from a 75–150 m. Lapôtre et al. (2016) did not explicitly estimate λ_0, but their histogram of bedform wavelengths observed by satellite on Mars (their Fig. 2B) has a minimum at a wavelength of 40 m, suggesting that λ_0 may be slightly larger than this minimum. Here we approximate λ_0 by a value of 100 m, keeping in mind this estimate may have an error of ±50 %.

Regardless of setting, the model results are scaled such that λ_0 is equal to 40 l_0, where l_0 is the elementary cell length (Zhang et al., 2014). Consequently, $l_0 = 0.5$ m on Earth, and approximately 2.5 m on Mars. The scales of the simulations in this paper are specified in the figure captions as multiples of l_0, and these lengths results can be expressed in meters by multiplying with the respective values of l_0 for Earth or Mars. Any errors in λ_0 or l_0 do not change the shape of the simulated dunes; they merely change their size.

As in nature, the sand flux in the model does not adapt immediately to the wind speed, and there is a distance, l_{sat}, required to reach saturation (Kennedy, 1969). In the simulations, this distance derives from the deposition length of an elementary cell mobilized by the flow, i.e., the typical distance required for an elementary particle to settle. Gao et al. (2014) have shown that $l_{sat} = 3\ l_0$. Interestingly, this approach gives a λ_0/l_{sat} ratio of about 13, which is close to the estimate based on observations and linear stability analysis (Elbelrhiti et al., 2005; Elbelrhiti, 2012; Lü et al., 2021).

The sediment transport capacity of the wind can also be controlled in the model. The transport capacity of our simulations is set so that it takes 1333 t_0 for a barchan of length 40 l_0 (40 $l_0 = \lambda_0$) to migrate a distance equal to its length, where t_0 is the characteristic time scale defined by Zhang et al. (2014) and matched with field observations of Elbelrhiti et al. (2005).

For the present study, we focused on two initial bed setups: (1) a thick sand layer under periodic boundary conditions; and (2) a conical sand pile on a non-erodible flat surface under open boundary conditions. Some simulations used a variant of the second setup, in which the initial sand pile was replaced with a sand source with a constant influx of sand. Those setups correspond to a fully sand-covered bed and a starved bed, respectively. Both kinds of beds were subjected to the same set of winds, which interacted with the evolving bed. Sand transport at each grid point was computed from the local wind conditions, and the local bed elevation was adjusted by the computed amount of deposition or erosion.

These setups thus approximate a broad spectrum of natural bed conditions: (1) a sand-covered bed on which dunes can grow as their crests accumulate sand from the bed while their troughs simultaneously

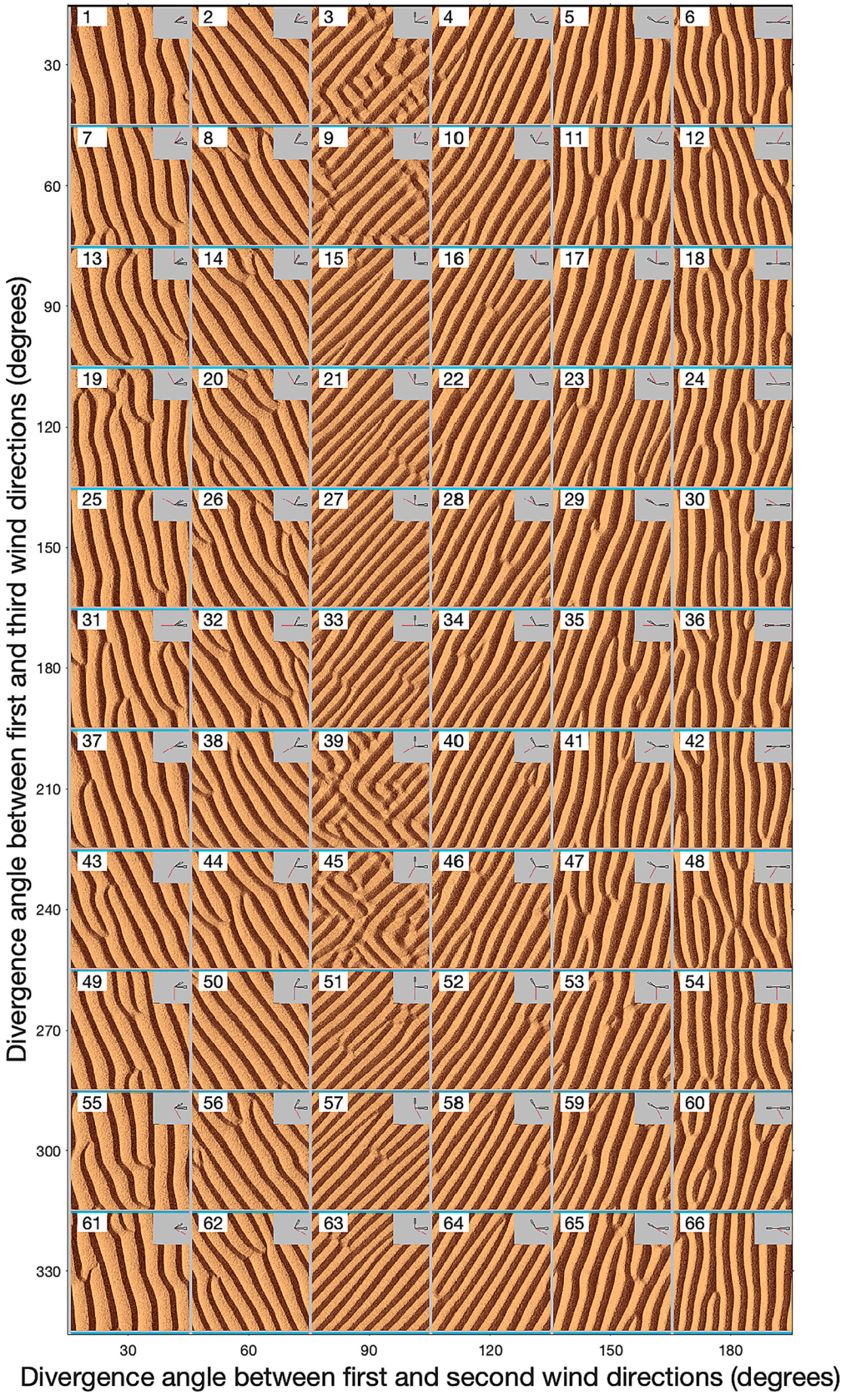

(caption on next page)

Fig. 1. Simulated dune morphology for winds blowing from three directions over a sand-covered bed. In all simulations, the dominant wind is directed toward the east, the secondary wind transports 75 % as much sand, and the third transports 10 % as much as the dominant wind. Because the weakest wind transports little sand relative to the other two, the wind regime approaches a bidirectional wind regime. The directions of the two weaker winds are defined relative to the dominant wind, measured in a counterclockwise direction. The divergence angle between the dominant wind and the secondary wind increases from 30° (left column) to 180° (right column); the divergence angle between the dominant wind and the weakest wind increases from 30° (top row) to 330° (bottom row). The sand-transport roses show the directional modes, with the most recent wind indicated in red. This is also the direction of the weakest wind as all snapshots are taken at the end of the wind cycle, which systematically goes from the strongest to the weakest wind. The resulting dunes have a single modal orientation, except in some wind regimes with orthogonal winds (cells 3, 9, 39, and 45). The dimensions of the cubic lattice of these simulations (height × width × length) is 60 l_0 × 500 l_0 × 500 l_0. The simulated wavelength is approximately 80 l_0, corresponding to 40 m and 200 m for terrestrial and Martian aeolian dunes, respectively. Images were recorded after 100 wind cycles. (For interpretation of the references to colour in this figure legend, the reader is referred to the web version of this article.)

scour into the underlying loose sand (2712 simulations using setup 1); (2a) a pile of sand that evolves into a dune while migrating over a non-erodible substrate (912 simulations using setup 2); in nature, dunes on a starved bed can either migrate into an area from upwind, or, alternatively, dunes on a sand-covered bed can evolve into isolated dunes as the dune field undergoes net erosion (outgoing sand exceeds incoming sand); and (2b) the variant of setup 2 where sand is supplied continuously at a localized source (1104 simulations). In nature, this localized source can be sand from upwind—including sand within upwind dunes on a starved bed. Results presented in this paper are from the first 2 setups, except that Fig. 5l, Fig. 6h and i use the variant with a localized source of sand. A detailed description of all simulations is provided in Rozier et al. (2024).

For each simulation, a predefined sequence of three winds and corresponding sand transport calculations was applied iteratively several hundred times. For the sake of completeness, we considered all possible pairs of divergence angles between the dominant wind and each of the two other winds, with a resolution of 30°. The three different winds in each simulation were allowed to transport very different amounts of sand, but to keep the number of simulations tractable, the secondary and ternary winds had relative durations chosen within the discrete set of ratios {1, 3/4, 1/2, 1/4, 1/10} with respect to the dominant wind. To vary the amount of sand transported toward different directions, the duration of each wind was set proportionately to the desired transport. We refer below to "weaker" winds, but, in fact, this term more precisely refers to winds of shorter duration. As a result, we simulated 900 tridirectional wind regimes (60 combinations of divergence angles for each of 15 combinations of transport ratios) plus a few extra bidirectional regimes occurring in some of the figures where the two weaker winds were toward the same direction.

Duration of each wind in each iteration was chosen such that the amount of sand transported during any step of each three-wind iteration was very small relative to the sand volume of the simulated dunes. This ensured that the final dune morphology accounted for all three vectors of the wind regime, rather than just the most recent wind, as illustrated diagrammatically by Rubin and Ikeda (1990). Many experimental and theoretical studies of bedforms in directionally varying flows have used this simplification because it avoids the complication of unsteadiness as dunes change shape or orientation with each flow pulse (Rubin and Hunter, 1987; Reffet et al., 2010; Courrech du Pont et al., 2015).

Although the duration of each iteration was small relative to the time to modify the dune, the overall number of wind cycles of each simulation was intended to be large relative to the number required to completely form or reshape the dune. One simulation that we are aware of (Fig. 6a) may not have attained this condition, because, as discussed in Section 4.2.3, morphology evolved throughout that simulation. In most simulations, however, the resulting morphology reflects all three winds (Bagnold, 1941; Gunn, 2023). The results presented in this paper are limited to the morphology at the end of each simulation, but movies illustrating evolution of each dune morphology through time are included in the archive described in Section 3.1. By limiting ourselves to the final simulated dune shapes, we voluntarily place ourselves in a context of extraterrestrial exploration in which it is rarely possible to have access to the long-term dynamics or knowledge of the different growth mechanisms responsible for the construction of dune patterns.

To avoid dunes on a starved bed migrating out of the computational space, that space moves with the center of mass of the sand. It was also expected that certain wind regimes in starved-bed conditions would produce elongated dunes, as reported by Rozier et al. (2019). To avoid dunes elongating out of the computational space, the wind regime for each simulation on a starved bed was oriented such that the resultant transport direction is parallel to the main axis of the system. Consequently, the orientations of all winds are rotated by an equal angle, but the divergence angles remain constant.

The model has two tunable parameters: the diffusion rate and the threshold for transport (Narteau et al., 2009). Two different values for each were investigated, but only for sand-covered beds. The diffusion rate controls sand transport perpendicular to wind direction, and accounts for the complicated processes of grain splashes and local wind redirection (Yizhaq et al., 2004). Here we report only present results of simulations using the lowest value of the diffusion coefficient and transport threshold for each of the bed setups, but the results for higher values of both parameters are included in the archive described in Section 3.1.

The approach to modeling taken here focuses on how the directional properties of a wind regime influence dune shape, whereas controls of dune size are largely avoided. Dunes can change size as they evolve, either by losing or trapping sand, perhaps growing until their height is limited by the amount of sand on the bed or limited by the thickness of the boundary layer (Andreotti et al., 2009), or perhaps until their height is limited by wind speed—if analogous to subaqueous dunes (Stein, 1965; Rubin and McCulloch, 1980; Zhang et al., 2010, Fig. 8). Modelling dune size is thus complicated because dune size can evolve through time. In contrast, many properties of dune morphology and orientation depend on symmetry or asymmetry of the wind regime, regardless of bedform size or fluid medium. For example, the flow property that controls the orientation of bedforms on sand-covered beds in bidirectional flows (maximized gross bedform-normal transport) was first identified in experiments with wind ripples (Rubin and Hunter, 1987), before being demonstrated to apply to subaqueous dunes (Rubin and Ikeda, 1990) or dunes in air (Ping et al., 2014). Consequently, focusing on shape rather than size leads to a more stable result of the simulations (i.e. shape stabilizes before size does), and the results are more broadly applicable.

This paper contains only a small subset of the 4728 simulations conducted for this study. Each of the first 4 figures contains the results of 66 simulations—including all specified combinations of divergence angles, but only a single pair of values of the transport ratio (out of 15 possible pairs). Considering the large number of simulations and the large number of calculations for each simulation, use of a supercomputer was essential.

3. Results

3.1. Data archive

Results of this work consist of 4728 simulated dune morphologies. Several hundred are presented here, to give a representative sample for the purposes of generalizing trends in morphology and interpreting dunes on Mars. To aid other work, all simulations are archived as both

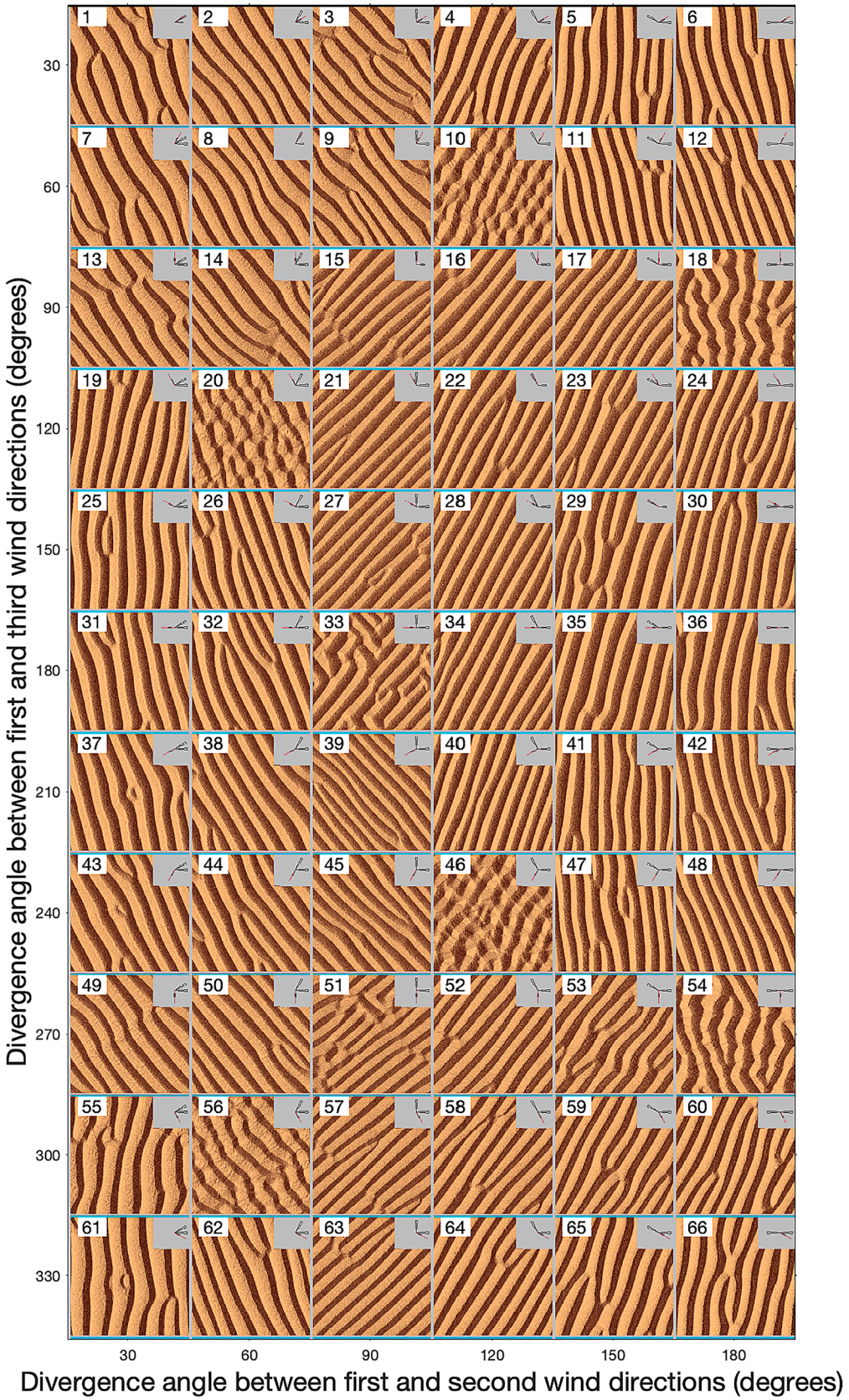

Fig. 2. Wind directions are the same as in the corresponding cell in Fig. 1, but the dominant and secondary winds transport equal amounts of sand, and the third transports 50% as much as the other two. Even the weakest wind transports a substantial amount of sand relative to the other two, so the wind regime is truly tri-directional. The sand-transport roses show the directional modes, with the most recent wind indicated in red. The resulting dunes have a single modal direction, except in some wind regimes with orthogonal winds (cells 33 and 51) and some regimes with winds diverging by 120° (cells 10, 20, 46, 56). Dimensions and number of wind cycles are the same as in Fig. 1. (For interpretation of the references to colour in this figure legend, the reader is referred to the web version of this article.)

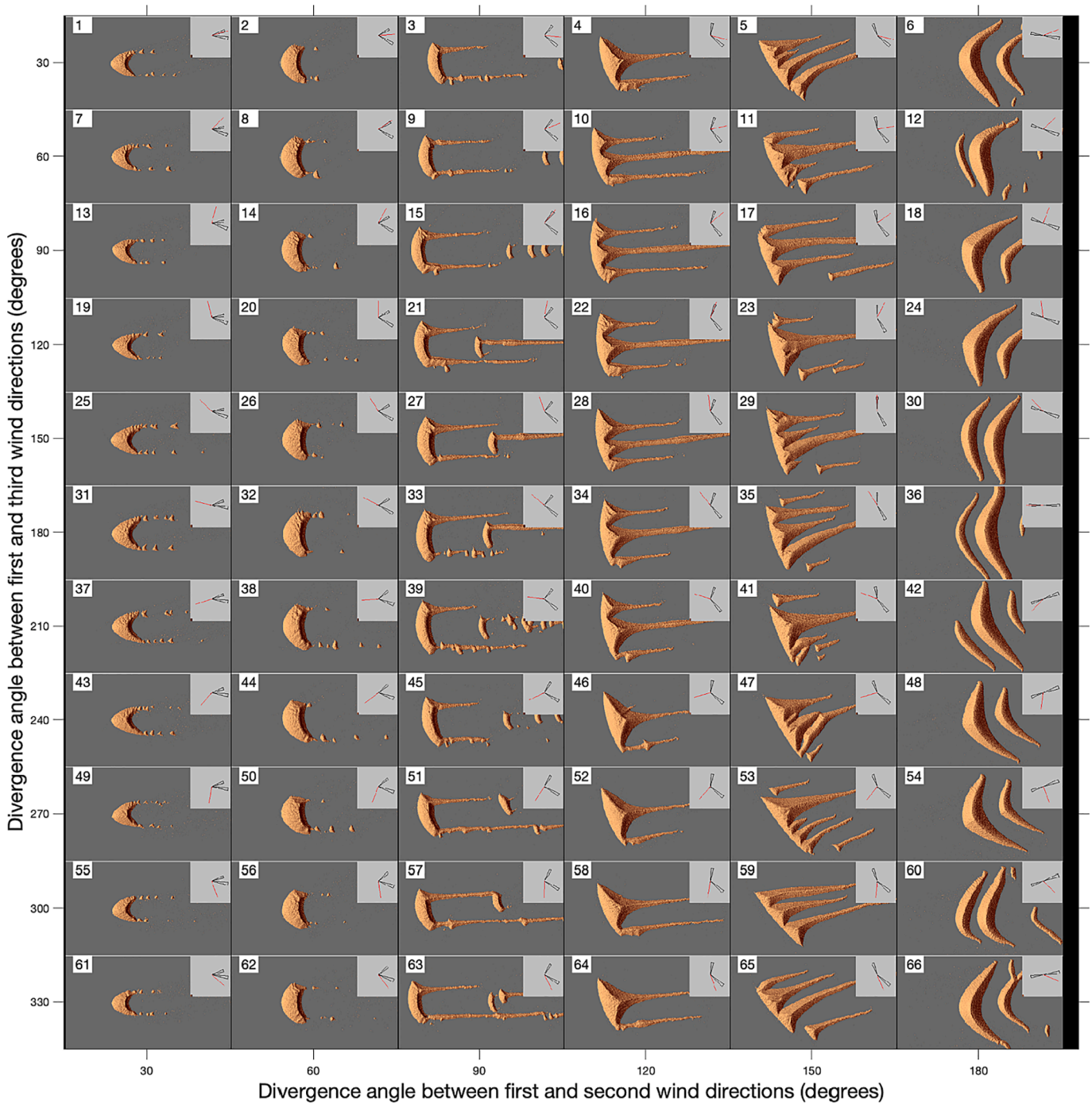

Fig. 3. Winds are identical to those in the corresponding cells in Fig. 1, but here the bed is partially starved. The weakest wind transports little sand relative to the other two, so the wind regime approaches a bidirectional wind regime. The sand-transport roses show the directional modes, with the most recent wind indicated in red. The resulting dunes generally change from symmetrical or asymmetrical barchans (left column) to squat barchans (second column from left) to "nail" dunes, and curved slug- or boomerang-shaped dunes (right column). The dimensions of the cubic lattice of these simulations (height × width × length) are 100 l_0 × 875 l_0 × 500 l_0 (corresponding to lengths and widths of 440 m × 250 m on Earth and 1000 m × 600 m Mars). The images were recorded after 300 wind cycles. (For interpretation of the references to colour in this figure legend, the reader is referred to the web version of this article.)

images of dune morphology and topographic files Rozier et al. (2024). Movies of the evolving dune morphology for selected simulations are also included in the archive.

3.2. Results of simulations

Although predicting dune morphology from a given wind regime and bed condition leads to a unique solution, many qualitatively similar morphologies or orientations can be produced by more than one wind regime—some wind regimes only slightly different and some grossly different from each other. The lack of uniqueness of solutions to this inverse problem is not the only difficulty in interpreting wind regime from dune morphology (Fernandez-Cascales et al., 2018); merely displaying and reviewing the thousands of images is difficult.

We compiled images showing the final dune morphology into grids (Figs. 1-4), in which the magnitudes of the three wind vectors remain

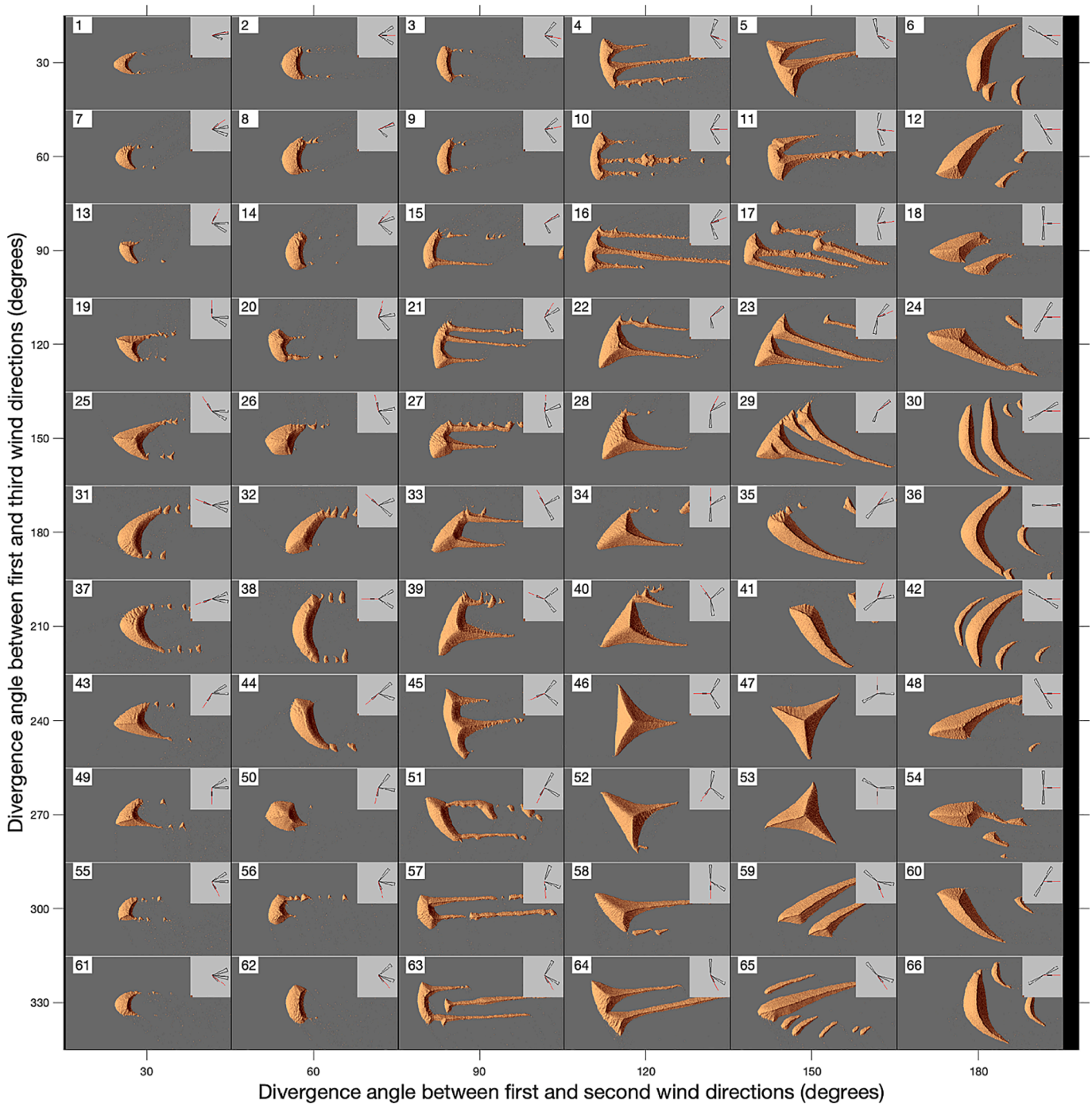

Fig. 4. Winds are identical to the corresponding cells in Fig. 2, but here the bed is partially starved. The sand-transport roses show the directional modes, with the most recent wind indicated in red. The weakest wind transports a substantial amount of sand relative to the other two, so the wind regime is truly tri-directional. Consequently, the resulting dune morphologies are more varied than in Fig. 3. Dimensions are the same as in Fig. 3. Images were recorded after 250 wind cycles. (For interpretation of the references to colour in this figure legend, the reader is referred to the web version of this article.)

unchanged within each figure, but the relative directions of the winds change systematically from cell to cell. The 66 cells in each of these figures are arranged such that the divergence angle of the second wind relative to the first (dominant) wind increases from 30° to 180° from left to right across the grid, and the divergence angle between the third wind (weakest) and the first increases from 30° to 330° from top to bottom. Thus, the wind directions in the corresponding cells in Figs. 1-4 are identical. The relative magnitudes of the winds, however, are not constant for all four figures. In Figs. 1 and 3, the transport ratios of the three winds are 1, 0.5, and 0.1 in every cell, whereas in Figs. 2 and 4, transport ratios of the three winds are 1, 1, and 0.5. Thus, the divergence angles and transport ratios of every cell in Fig. 1 are identical to those of the corresponding cell in Fig. 3, and divergence angles and transport ratios of every cell in Fig. 2 are identical to the corresponding cell in Fig. 4.

4. Discussion

4.1. Approach

This Discussion has five parts. Section 4.1 discusses the approach in generalizing the results, Section 4.2, discusses simulated morphologies on sand-covered beds, Section 4.3 discusses morphologies on starved

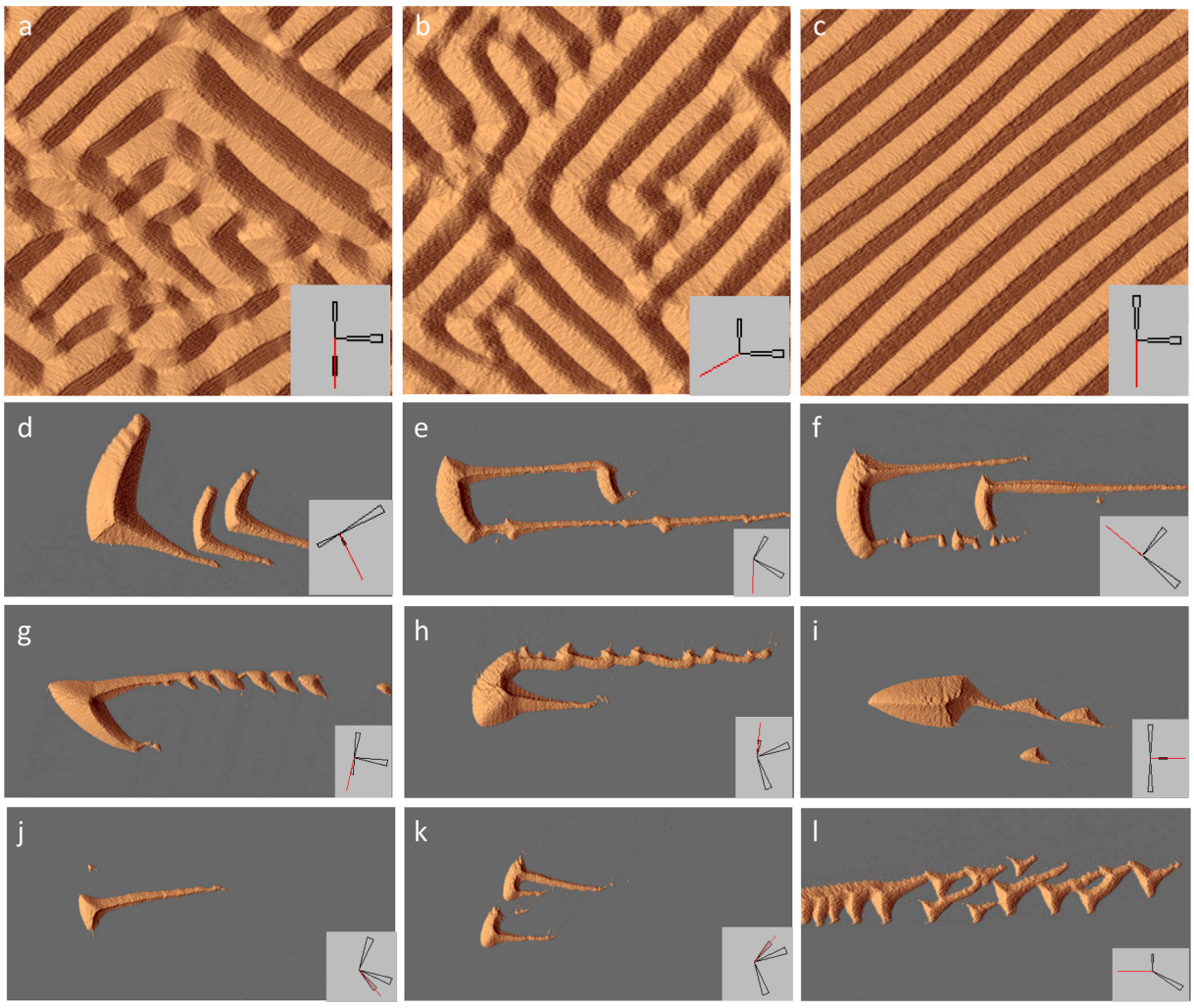

Fig. 5. Simulated dunes in orthogonal wind regimes. The sand-transport roses show the directional modes, with the most recent wind indicated in red. (a-b) Maze-like dune patterns on sand-covered beds. Neither of the two dune orientations is perpendicular to any wind mode, as is commonly inferred. (c) Linear dunes formed parallel to the resultant transport direction (i.e., longitudinal dunes). (d-f) Isolated dunes with crests having two orthogonal orientations. No dune orientations are perpendicular to any of the wind modes; rather, crest orientations are oblique to individual wind modes. (g) Asymmetrical barchan with one long arm consisting of a chain of asymmetrical barchan-like dunes, formed in asymmetrical orthogonal wind regime. (h) Asymmetrical barchan with a long arm consisting of a chain of peaks and saddles. (i) Barchan-like dune formed in symmetrical wind regime with two strong and one weak orthogonal wind. Simulations by Parteli et al., (2009, Fig. 3) produced similar morphology in bidirectional flows with a divergence angle of 160°. (j) "Nail" dune with long tail. (k) "Nail" dunes with shorter tails. (l) "Nail" dunes transitional with star dunes. Sand was supplied continuously at a fixed location. Fig. 5a-c have horizontal dimensions of 500 l_0 × 500 l_0 and 100 wind cycles. Fig. 5d-k have dimensions 875 l_0 × 500 l_0 and 250 wind cycles. Fig. 5l has dimensions of 776 l_0 × 388 l_0 and 300 wind cycles. l_0 is 0.5 m on Earth and 2.5 m on Mars. (For interpretation of the references to colour in this figure legend, the reader is referred to the web version of this article.)

beds, Section 4.4 lists factors that the simulations did not explore, and Section 4.5 compares examples from Mars with the analogous simulated morphologies.

For a given bed subjected to tri-directional wind regimes, dune morphology is determined by six independent variables: the magnitudes and directions of the three wind vectors. We can reduce this to four independent variables by defining the magnitudes and directions of two vectors relative to the third; here we define the two weaker winds relative to the strongest. The results in Figs. 1-4 thus represent 2-dimensional slices through this 4-dimensional parameter space—slices in which the magnitudes of the three wind vectors remain constant for all 66 cells in each figure.

The following discussion generalizes trends in dune morphology as the divergence angles change. The strongest winds exert the greatest control on morphology, so the discussion emphasizes how morphology changes as the divergence angle between the two strongest winds increases from 30° to 180°. The generalized morphologic sequence is, by necessity, rather imprecise, however, because it follows changes in a single independent variable (divergence angle between the two dominant winds).

The most obvious control of dune morphology in the thousands of simulations is that dunes on a sand-covered bed (Figs. 1 and 2) tend to form long crests with relatively uniform orientations, whereas dunes on a starved bed have a greater diversity of crest orientations and shapes, including complex shapes (Figs. 3 and 4) that have not been simulated or observed in bidirectional wind regimes. The specific dune shapes resulting from the tri-directional wind regime persist regardless of whether the transport capacity of the weakest of the three winds is a substantial fraction or only 1/10th that of the dominant wind.

4.2. *Sand-covered beds*

4.2.1. *General trends*

On sand-covered beds, dune orientation varies qualitatively as expected from the previous work discussed in Section 1.2. In approximately bidirectional winds, dune orientation abruptly jumps from a

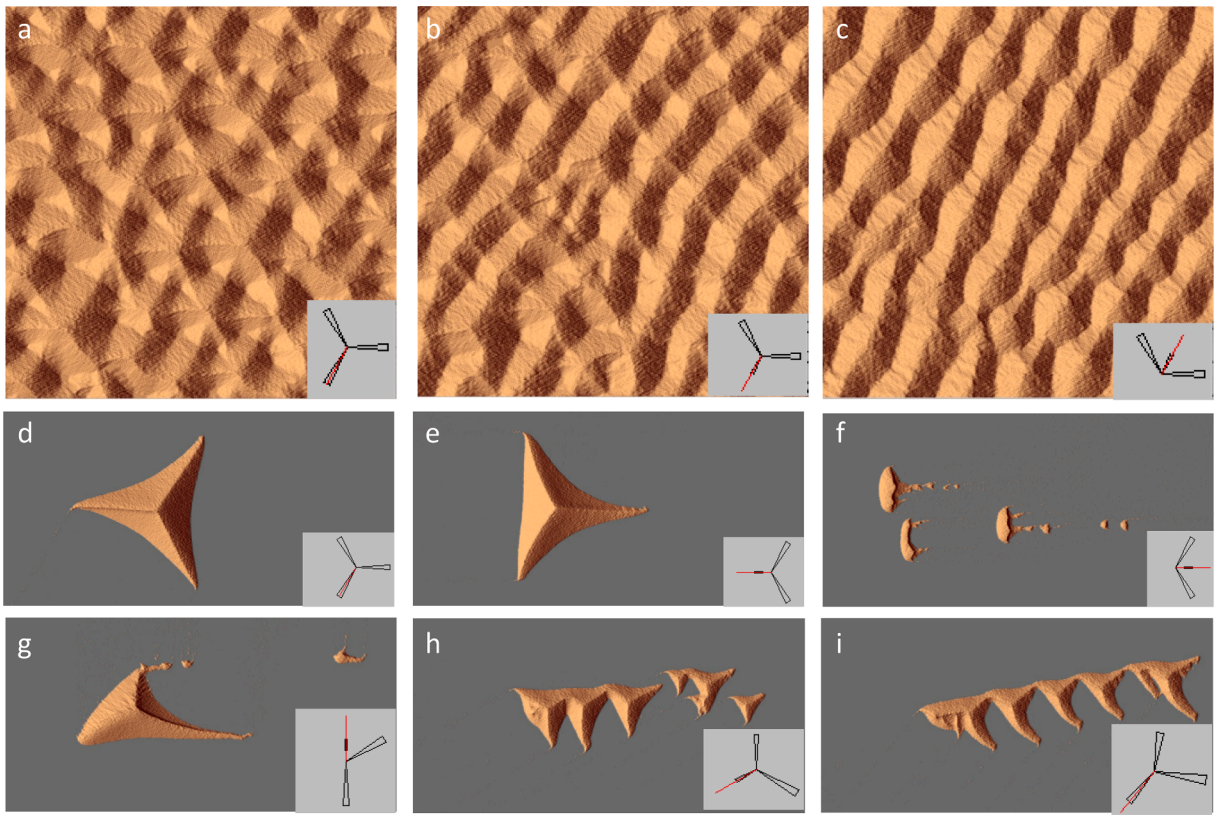

Fig. 6. Simulated dunes on sand-covered beds (a-c) and starved beds (d-i) in wind regimes with varying degrees of triradial symmetry. The sand-transport roses show the directional modes, with the most recent wind indicated in red. (a) Winds with perfect triradial symmetry produce three intersecting sets of crests and chains of star dunes with triradial symmetry. (b) One of the three winds is weaker than the others, generating only two crest orientations. (c) The same wind regime as in (b) except that the weaker wind is reversed. Only two crest orientations or lineations are produced. (d) Symmetrical star dunes formed in a wind regime with the same triradial symmetry as in (a). (e) One wind mode is weaker than the other two (same wind regime as (b)), causing one arm of the star to become longer and skinnier than the other two. (f) Reversing the direction of the weaker wind causes the star dune to convert to a dome with a tail (same wind regime as (c)). (g) Asymmetrical shark-tooth-shaped dunes (https://www.jpl.nasa.gov/images/pia03208-sharks-teeth-sand-dunes-in-proctor-crater) formed where one of the three wind modes is weaker and rotated from the radially symmetrical orientation. This morphology is similar to the "raked linear dunes" that require three wind modes, as shown by Lv et al. (2017). (h) Clusters of star dunes formed in wind regime where wind modes are separated by 120° but unequal in magnitude. Sand was supplied continuously at a fixed location. (i) Chain of shark-tooth-shaped dunes formed where one of the three wind modes is rotated 30° from radial symmetry. Sand was supplied continuously at a fixed location. Fig. 6a-c have horizontal dimensions of 500 l_0 × 500 l_0 and 100 wind cycles before the images were recorded. Fig. 6d-g have dimensions of 875 l_0 × 500 l_0 and follows 250 wind cycles. Fig. 6h has dimensions of 968 l_0 × 484 l_0 and 300 wind cycles. Fig. 6i has dimensions of 896 l_0 × 448 l_0 and follows 300 wind cycles. l_0 is 0.5 m on Earth and 2.5 m on Mars. (For interpretation of the references to colour in this figure legend, the reader is referred to the web version of this article.)

generally transverse orientation (columns 1 and 2 on the left side of Figs. 1 and 2) to longitudinal or oblique orientations on the right side (columns 4–6). Dunes on the left sides of Figs. 1 and 2 experience sand transport that is primarily in one direction across each crest (left to right) and, consequently, those dunes are asymmetrical in cross-section. Asymmetry is demonstrated by the wider stoss sides (light-toned) and narrower lee sides (darker). In contrast, dunes on the right sides of those figures experience substantial transport from both directions across their crests and are more symmetrical in cross-section, as indicated by the more uniform widths of their two flanks. This overall pattern across the cells in Figs. 1 and 2 is consistent with the previous studies cited in Section 1.2 that found that dunes on sand-covered beds took orientations having the maximum gross across-crest transport, although we didn't conduct a detailed comparison of observed and predicted orientations.

In any one simulation, dunes on a sand-covered bed generally have a single modal orientation, except in special cases where winds diverge by 90° or 120°. These special wind regimes produce dunes with more than one modal orientation, as discussed in the following two sections. Because many combinations of two or three winds can create dunes with relatively continuous crests with few distinctive properties, the inverse problem of identifying what wind regime produced this simple kind of dune may have no unique solution, although the observed across-crest symmetry/asymmetry may indicate whether the formative wind regime more closely matches those on the left or right sides of Figs. 1 and 2.

4.2.2. Special case where gross bedform-normal transport has two approximately equal maxima (geometrically orthogonal winds)

At a divergence angle of approximately 90° the between two dominant winds, simulated dunes on a sand-covered bed may develop two crest orientations (Figs. 1.3, 1.9, 1.39, 1.45; Figs. 2.33 and 2.51; Fig. 5a and b). This result is consistent with previous studies of bidirectional flows that have found a discontinuity in orientation at a divergence angle of ~90° (Rubin and Hunter, 1987; Rubin and Ikeda, 1990; Werner and Kocurek, 1997; Parteli et al., 2009; Reffet et al., 2010; Courrech du Pont et al., 2014; Gao et al., 2015a, 2015b). At this transition, the two orientations have been observed as either an intersecting pattern (Reffet et al., 2010, Fig. 1B and D), or as a maze-like pattern (Nishimori and Tanaka, 2003, Fig. 3C and D; Reffet et al., (2010, Fig. 2E) where individual crests make 90° bends (Fig. 5a and b).

Where dunes have two orientations in approximately bimodal winds (Figs. 1.9, 1.39 and 1.45), one of the two orientations is approximately normal to the resultant transport direction; transport across dunes with

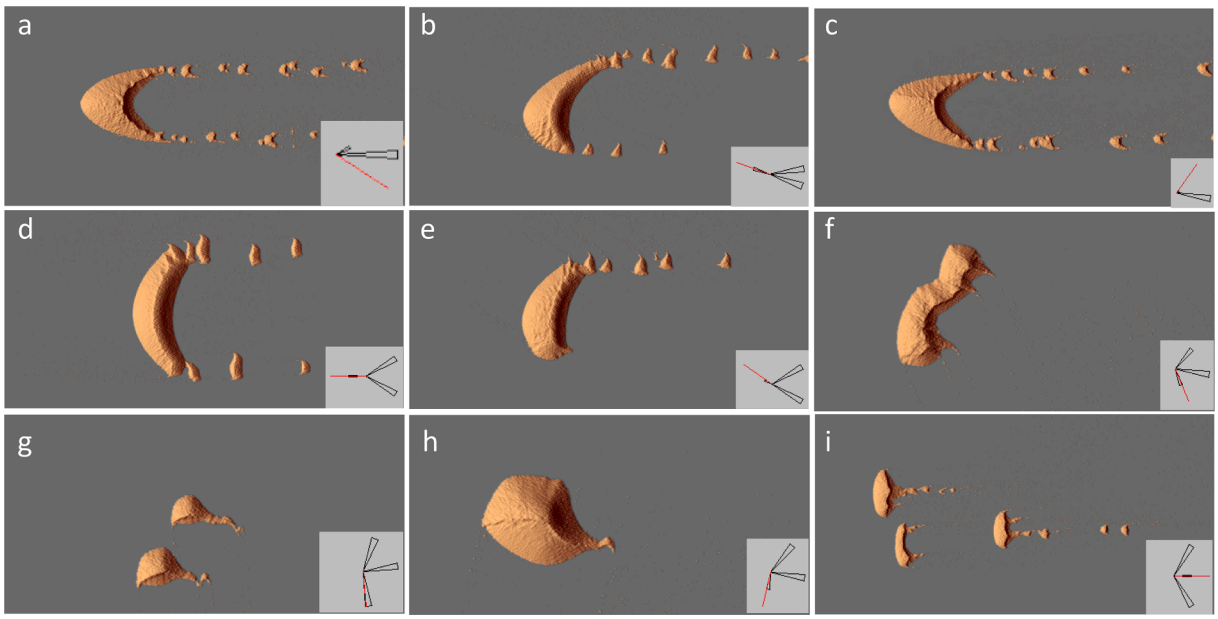

Fig. 7. Barchan and dome-like dunes formed on partly starved beds. Horizontal dimensions are 875 l_0 × 500 l_0; 250 wind cycles. (a) Symmetrical barchan. (b) Asymmetrical barchan formed in asymmetrical tri-directional wind regime. (c) Asymmetrical barchan formed in a wind regime with one dominant mode and two weaker modes. (d) Symmetrical squat barchan in a symmetrical wind regime. Divergence angle between the two dominant winds is 60°, which is greater than for classic barchans. (e) Asymmetrical squat barchan. The two dominant modes are the same as in (d), but the third (weakest) mode is asymmetrically oriented. (f) Laterally linked squat barchans. (g-i) Asymmetrical domes with tails.

this orientation is consistently from one side of the dune to the other. The second orientation has approximately equal gross bedform-transport to the first, but transport reverses across the dune crests. Where the two transport modes are equal in magnitude, this second orientation is approximately parallel to the resultant transport direction, but this alignment is coincidental, rather than the cause of the second orientation, as shown by Rubin and Hunter (1987) and many of the subsequent studies cited in section 1.2.

The discontinuity in dune orientation observed at a 90° divergence angle between two dominant winds (for example, between the left and right sides of Figs. 1 and 2) is consistent with previous work, although the precise divergence angle at which the discontinuity occurs was found to vary slightly: 90° (Rubin & Hunter, 1987; Rubin & Ikeda, 1990; Courrech du Pont et al., 2014; Gao et al., 2015a), 90° – 110° (Werner and Kocurek, 1997, Fig. 4), and 80° – 90° (Reffet et al., 2010). The two orientations that arise in our simulations at a divergence angle of 90° are the two orientations that occur in conditions on either side of this phase boundary. In approximately bidirectional flows with a divergence angle of 90° (Fig. 1, column from 1.3 to 1.63), however, some simulations show only a single dune orientation. In these cases, the single orientation is consistently the orientation that is more longitudinal rather than the transverse orientation. This result agrees with the experimental results of (Reffet et al., 2010), who reported the phase change to occur at a divergence angle of 80° – 90°.

4.2.3. Special case of winds with triradial symmetry

Just as a wind regime with two orthogonal winds can produce two dune orientations, a wind regime with triradial symmetry (three equal winds with divergence angles of 120° and 240°) produces a network of three intersecting crest trends (Fig. 6a). This unique situation is one where dune morphology evolved throughout the simulation (as illustrated by the movie in the archive). This wind regime nevertheless appears to be another example where none of the individual crest orientations are perpendicular to a corresponding wind direction (Fig. 6a).

As the wind regime becomes less symmetrical—either because the winds rotate or because they become unequal in magnitude—the symmetry of the triradial dune morphology degrades (Fig. 6b and c). A special case occurs where one of the three winds is reversed from the radially symmetric orientation. In this case only two of the three orientations are retained (Figs. 2.10, 2.20, 2.56, Fig. 6f). Section 4.3.3 discusses analogous morphologies of these dunes to those in identical triradial wind regimes on a starved bed.

4.3. Starved beds

4.3.1. Barchan and barchan-like dunes (most transport restricted to within approximately 30° or 60°)

On a starved bed, the simulations generate barchans where trimodal winds crudely approximate unidirectional winds, such as where two dominant winds diverge by only 30° (simulations along the left edge of Fig. 3) or where the weaker modes transport only a small fraction of the total transport (Fig. 7a). Barchans are relatively symmetrical in planform where two weak winds are symmetrically distributed relative to the dominant wind or where they transport only a small proportion of the total transport. As the weaker winds become more substantial, barchans can become more asymmetric; for example, asymmetry in Figs. 4.25 and 4.43 is much greater than in Figs. 3.25 and 3.43. Such asymmetric barchans are common on Earth and Mars, as was discussed in Section 1.2.

As the divergence angle between two substantial wind modes increases from 30° to 60°, barchans become squatter, with stubby horns (Fig. 3, column of simulations from 3.2 to 3.62; Fig. 7d and e), resembling the “rounded” or “oblate” barchans that Parteli et al. (2014) created in similar simulated winds. Asymmetry in these two dominant wind modes leads to asymmetric morphology, in this case retaining the squatter morphology (Fig. 7e), or barchanoid ridges with more continuous crests (Fig. 7f). Dunes with these morphologies here are common on Mars, as illustrated below in Section 4.5. As a greater proportion of the total transport occurs over a wider range of directions, dune morphology evolves to include domes, some with curved tails (Figs. 4.13, 4.50 and 4.55; Fig. 7g and h), as shown previously by Gao et al., (2018, Figs. 2 and 4B).

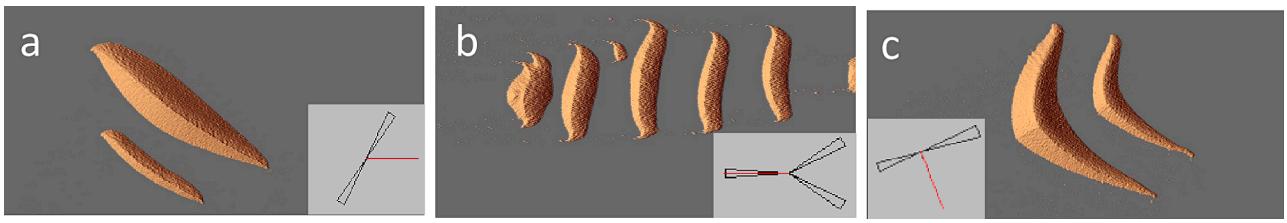

Fig. 8. Slug- and boomerang-shaped dunes formed in reversing wind regimes. Horizontal dimensions are 875 l_o × 500 l_o; 300 wind cycles. (a) The two dominant winds are equal in magnitude but opposite in direction, and the third is very weak, producing relatively straight-crested dunes. Martian dunes with this shape are commonly called "transverse aeolian ridges" or "TARs", but in this example the dunes are oblique to net transport rather than transverse. The two dominant winds are diametrically opposed and thereby cancel out; net transport is determined uniquely by the third (weak) wind. (b) Three equal winds with lateral symmetry produce relatively straight-crested dunes. The dunes are roughly transverse to the resultant transport direction, but two winds blow from right to left and only one from left to right, producing cross-sectional asymmetry with a wider, gentler stoss side (facing right) and steeper lee side (facing left). Sand was supplied at a point. (c) Boomerang-shaped dunes formed by two strong but unequal reversing winds and a much weaker orthogonal wind.

4.3.2. Dunes in geometrically orthogonal winds (divergence angles of ~90°)

On a starved bed in a wind regime where the two dominant wind modes increase from an acute angle to 90°, dunes change from barchans (column 1 in Figs. 3 and 4) or squat barchans (column 2 in Figs. 3 and 4) to "nail" dunes (Song et al., 2019; Chao and Zhibao, 2022) (columns 3–5 in Figs. 3 and 4). Differences in the magnitude of the orthogonal wind modes—or addition of a third mode—causes asymmetric morphology, as illustrated in Figs. 3.63 and 4.21. In a wind regime with two or more orthogonal modes, barchan-like asymmetry can be particularly pronounced, with one very long arm resembling a sinuous linear dune (Fig. 5g – i). This is reminiscent of the dunes elongating from a topographic obstacle (Lucas et al., 2015).

4.3.3. Dunes in winds with triradial symmetry (divergence angles of 120° and 240°)

In our simulations, a triradially symmetrical wind regime on a starved bed produces star dunes with three arms (Fig. 6d), as reported previously by Zhang et al. (2012). As noted in Section 4.2.3, the identical wind regime on a sand-covered bed produces a triradially symmetrical pattern of intersecting crests (Fig. 6a) rather than isolated stars. These two morphologies (Fig. 6a and d) arise in the identical wind regime, and both have triradial symmetry; the different morphologies result purely from the differing sand coverage on the bed.

As the wind regime loses its symmetry star dunes lose their symmetry. In some cases, one of the three radial arms becomes elongated, resembling a shark's tooth (Fig. 4.34; Fig. 6g – i). Similar morphologies have been reported in wind regimes with three modes in simulations and on deserts on Earth (Lv et al., 2017). In other cases, crests that roughly parallel the resultant transport direction become more pronounced (Figs. 3-40).

4.3.4. Dunes in reversing winds (divergence angles of ~180°)

As the divergence angle between two dominant wind modes increases to 180°, the wind regime approximates a reversing flow, analogous to those that produce reversing tidal dunes or oscillatory ripples under waves. The dunes simulated on a starved bed in these flows have a relatively distinctive shape (cells along the right edge of Figs. 3 and 4; Fig. 8), resembling a boomerang (Fig. 3.6) or slug (Fig. 3.42). Simulations by Parteli et al., (2014, Fig. 4c) produced dunes with similar morphology in bidirectional wind regimes with a divergence angle of 160°.

4.4. Unexplored issues

Despite the large number of simulations conducted in this study, many unknowns remain. We haven't explored how dune morphology evolves through time. Specifically, in simulations that begin with a conical sand pile (such as Figs. 3 and 4), the amount of sand decreases through time. Previous work has suggested that duration of each flow cycle can influence the resulting morphology (Parteli et al., 2014), although the reported changes are typically changes in length and width of dune features rather than a change from one kind of dune to another. Inspection of a small subset of our simulations is consistent with this observation. To avoid the complication where dune morphology changes with each pulse of wind, we have restricted the simulations to flows where individual wind pulses transport an amount of sand that is small relative to dune volume. Not all natural flows have this property.

We haven't modified the dune simulation model to account for Mars atmosphere, sediment density, or gravity, and we don't know if dune morphology varies systematically between Earth and Mars. Several factors suggest that this is not a serious issue for our purposes. First, because the ratio of transport toward different directions is adjusted by the duration of the winds rather than their magnitudes, the results aren't affected if the transport rates are all greater or less than calculated. Second, many of the factors influencing dune morphology are related to symmetry or asymmetry of winds, which remain constant even if all wind vectors are too great or small by a constant proportion.

We have not explored which lateral diffusion coefficient is most appropriate, and the simulations have only focused on forward modeling: what dunes a given wind regime will produce. We have not addressed the inverse problem of inferring wind regime from an observed morphology. We encourage the use of this archive of simulations for further comparative geomorphology and training of algorithms for the inverse problem of interpreting wind regimes from dune morphology.

4.5. Examples from Mars

Our simulations generated a wide range of dune morphologies, many of which are present on Mars. We present below a sample of these morphologies. We cannot prove that the dunes on Mars formed by the same wind regime that produced a similar morphology in the simulations, because more than one wind regime can produce similar morphologies. In addition, other factors that were not examined in the simulations—such as sediment cohesiveness—are known to be important in influencing dune morphology (Schatz et al., 2006; Rubin and Hesp, 2009). Nevertheless, the simulated wind regimes that produce a simulated morphology are a reasonable working hypothesis for what wind regime produced an observed dune form in nature. Although the examples presented are all from Mars, many of the same morphologies occur on Earth—including some of the more unusual forms, such as nail dunes (Song et al., 2019).

4.5.1. Barchan and barchan-like dunes

Many of the barchan and barchan-related morphologies produced in the simulations (Figs. 3, 4 and 7) also occur on Mars (Fig. 9). For example, dunes on Mars include classical, symmetrical barchans (Fig. 9a

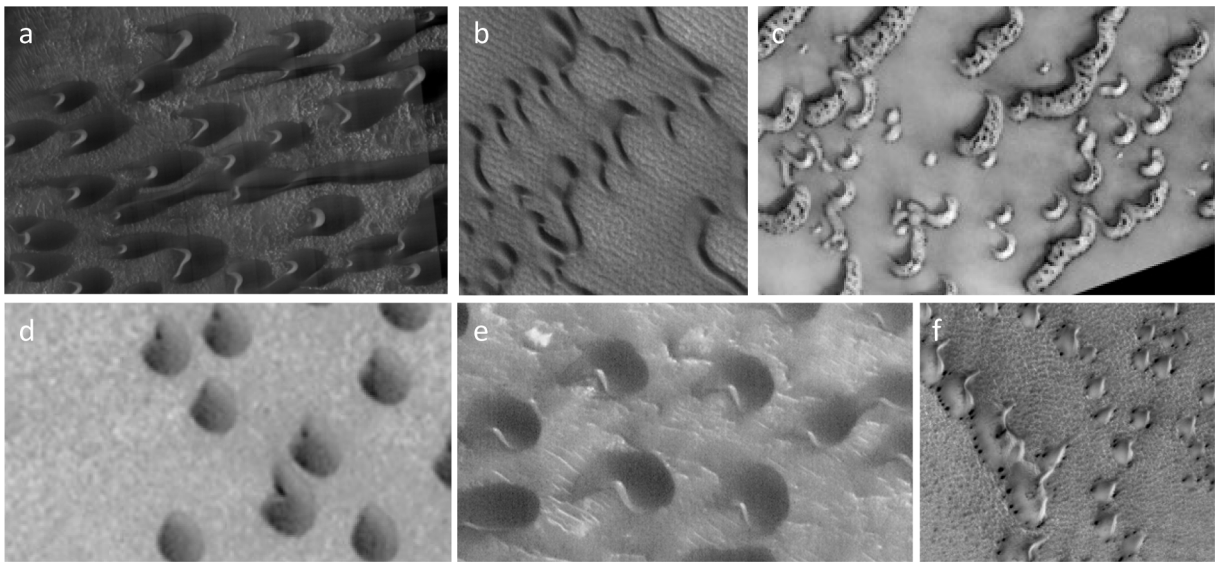

Fig. 9. Barchan and dome dunes on Mars. (a) Symmetrical barchans. (b) Asymmetrical barchans. (c) Squat barchans. (d-e) Asymmetrical domes. (f) Domes with tails. Images a, c, f: NASA/JPL-Caltech/UArizona; images b, d, e: NASA/JPL/Malin Space Science Systems.

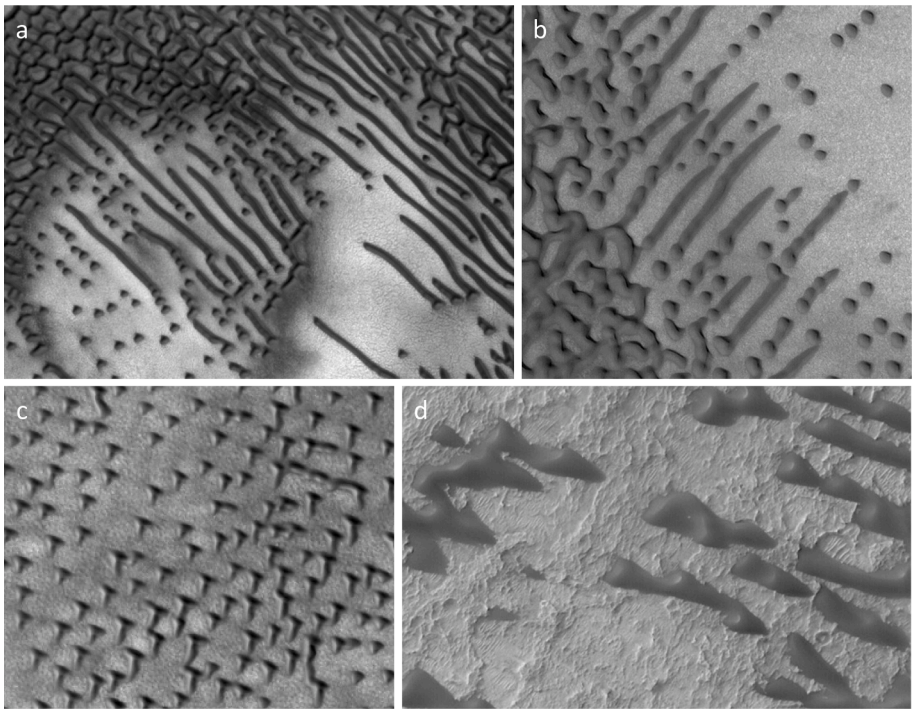

Fig. 10. Dunes inferred to have formed by orthogonal wind regimes on Mars. (a-b) Maze-like patterns with orthogonal crest orientations. (c) "T" or "nail" dunes. (d) Dune resembling simulation shown in Fig. 5i. Images a, c: NASA/JPL-Caltech/UArizona; images b, d, NASA/JPL/Malin Space Science Systems.

resembling those in Fig. 7a), asymmetrical barchans (Fig. 9b resembling Fig. 7b and c), squat barchans (Fig. 9c resembling Fig. 7d – f), and a variety of dome-like forms (Fig. 9d – f resembling Fig. 7g – i), including domes with tails (Fig. 9f resembling Fig. 7i). We presume that the dunes on Mars were formed in wind regimes resembling those of the corresponding simulations.

4.5.2. *Dunes in orthogonal winds*

Dunes on Mars include a variety of morphologies resembling those that are arise in simulations with wind regimes that have approximately orthogonal wind directions. These morphologies include maze-like forms with orthogonal crest orientations (Fig. 10a and b crudely resembling Fig. 5a and b), "nail" dunes (Fig. 10a – c resembling Fig. 5j – l), and dunes that appear to be a hybrid of barchans and linear dunes with sinuous crests (Fig. 10d resembling Fig. 5i).

4.5.3. *Dunes in wind regimes with triradial symmetry*

Many of the simulated morphologies that form in winds with triradial symmetry occur on Mars (Fig. 11), on both starved beds and sand-covered beds. Morphologies on a starved bed include star dunes (Fig. 11a and b) and chains of linked dunes with shark-tooth shape (Fig. 11c). It is unclear whether this latter morphology belongs to the class of dunes formed by approximately triradial winds (as in Fig. 6i) or whether it is more closely related to dunes formed in orthogonal winds

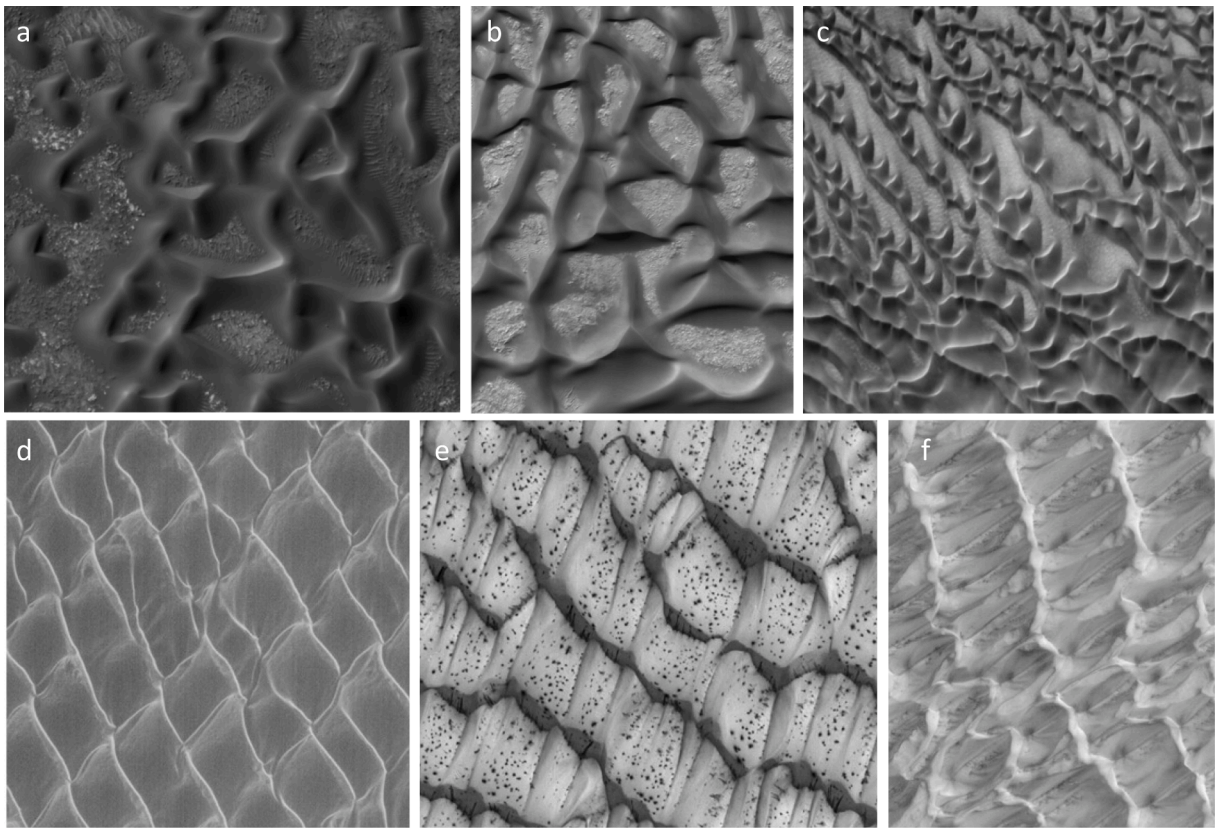

Fig. 11. Dunes with morphology suggesting triradial wind regimes. (a-b) Star dunes. (c) Chain of shark-tooth-shaped dunes resembling simulations in Figures 5g and 6i. (d-f) Oblique intersecting patterns resembling simulations in Figures 2.10, 2.20, 2.46, 2.56, and 6b-c. Images a, c: NASA/JPL-Caltech/UArizona; images b, d, e, f: NASA/JPL/Malin Space Science Systems.

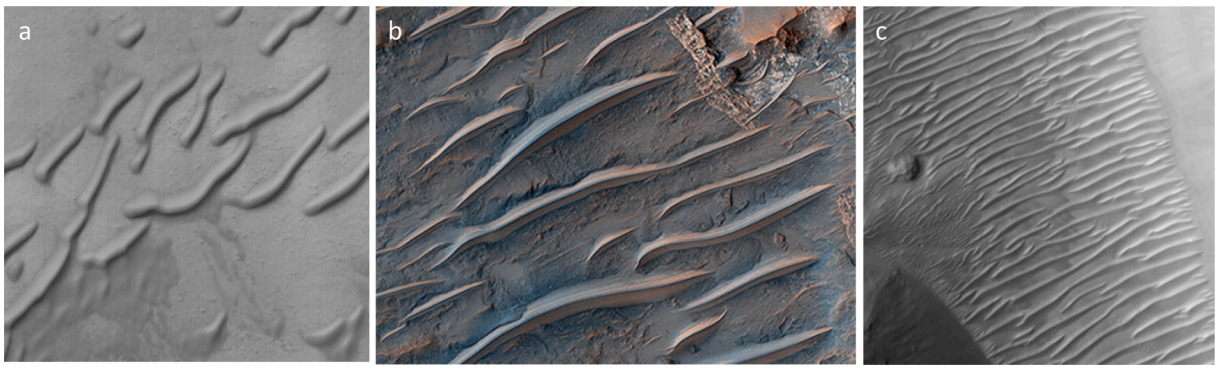

Fig. 12. Dunes on Mars with morphology resembling simulated dunes in reversing winds. Images: NASA/JPL/Malin Space Science Systems.

(as in Fig. 5g). Morphologies resembling those formed by simulated triradial winds also occur on sand-covered beds on Mars (Fig. 11d – f resembling Fig. 6b and c).

4.5.4. Dunes in reversing winds

In the simulations, reversing winds produce relatively straight-crested dunes (Fig. 8), as is typical of bedforms in reversing aeolian and subaqueous flows (Rubin, 2012). Aeolian bedforms with this morphology are ubiquitous on Mars (Fig. 12) and commonly referred to as "transverse aeolian ridges" or "TARs" (Zimbelman, 2010; Geissler and Wilgus, 2017). The term "TAR" can be misleading because the crests of these bedforms—like the crests of wave ripples, tidal dunes, and other straight-crested bedforms in reversing flows—need not be oriented transverse to the net transport direction (Rubin, 2012), which is key to distinguishing transverse, oblique and longitudinal dunes as defined by Hunter, Richmond, and Alpha (1983). Where the two strongest winds are equal in magnitude and diametrically opposed, dunes can form with an orientation that is approximately perpendicular to those winds, but because transport from those two winds has a net transport of zero, even a weak wind from any other direction determines the net transport direction. Similarly, where two winds transport equal amounts of sand but diverge by an angle that differs slightly from 180°, the resulting dunes will lie parallel to the resultant. In these two situations, dunes can be oblique, parallel, or transverse to the resultant sand transport direction, depending on the orientation of dune relative to net transport. Although dunes in these two situations form approximately perpendicular to the two individual dominant winds, they do not meet Hunter, Richmond, and Alpha's definition of "transverse" unless the net transport direction is approximately perpendicular to the dune crest.

Table 1
Examples of Mars dunes with morphologies resembling simulated dunes.

Figure	HiRISE image	Corresponding simulations	Other HiRISE images with similar dune morphologies
9a	https://hirise-pds.lpl.arizona.edu/PDS/EXTRAS/RDR/ESP/ORB_076200_076299/ESP_076221_1380/ESP_076221_1380_RED.browse.jpg	Fig. 7a; symmetrical morphologies in left column of Fig. 3	
9b	https://www.msss.com/mars_images/moc/2005/01/06/	Fig. 7b and c; asymmetrical morphologies in left column of Figs. 3 and 4	https://www.msss.com/mars_images/moc/2004/07/20/ https://hirise-pds.lpl.arizona.edu/PDS/EXTRAS/RDR/ESP/ORB_026800_026899/ESP_026839_2550/ESP_026839_2550_RED.browse.jpg
9c	https://www.uahirise.org/ESP_034441_2565	Fig. 7d – f; second column from left in Figs. 3 and 4	https://www.uahirise.org/ESP_024881_2560 https://www.msss.com/mars_images/moc/2004/07/27/ https://www.msss.com/mars_images/moc/2004/05/31/ https://www.msss.com/mars_images/moc/2004/01/10 https://www.msss.com/mars_images/moc/2003/09/26/
9d	https://www.msss.com/mars_images/moc/2003/07/25/	Figs. 4.50 and 7h	
9e	https://www.msss.com/mars_images/moc/2003/08/16/	Figs. 4.50 and 7h	
9f	https://www.uahirise.org/ESP_024265_2535	Fig. 7i and 4.10 (after additional iterations	https://www.msss.com/mars_images/moc/2004/10/22/ https://www.uahirise.org/ESP_024505_2555
10a	https://www.uahirise.org/ESP_044675_2580	Figs. 4.15–4.17, 4.57, 4.63, 5j and k	
10b	https://www.msss.com/mars_images/moc/2004/11/09/	Figs. 4.15–4.17, 4.57, 4.63, 5j and k	
10c	https://www.uahirise.org/ESP_062151_2540	Fig. 5j – l [lower case L]	
10d	https://www.msss.colo nm m/mars_images/moc/2003/06/14/	Fig. 5i	
11a	https://www.uahirise.org/ESP_059292_1310	Fig. 6h	
11b	https://www.msss.com/mars_images/moc/2004/08/21/	Fig. 6h	
11c	https://www.uahirise.org/ESP_044853_2580	Fig. 5g and i	
11d	https://www.msss.com/mars_images/moc/2004/04/14	Fig. 6b and c	
11e	https://www.msss.com/mars_images/moc/2004/08/23	Fig. 6b and c	
11f	https://www.msss.com/mars_images/moc/2006/05/08	Fig. 6b and c	
12a	https://www.msss.com/mars_images/moc/2004/06/28/	Fig. 8	
12b	https://www.uahirise.org/ESP_020782_1610	Fig. 8	
12c	https://hirise-pds.lpl.arizona.edu/PDS/EXTRAS/RDR/ESP/ORB_046500_046599/ESP_046592_1520/ESP_046592_1520_RED.browse.jpg	Fig. 8	

5. Conclusions

The thousands of dune morphologies simulated in this study encompass a wide variety of forms found on Mars (Table 1). Many of the morphologies vary gradually across a spectrum of morphologies as the magnitudes and directions of the two or three wind modes change. The simulations can be used to guide the interpretation of what wind regimes produce a given morphology, although some morphologies can form in different regimes.

On a sand-covered bed most wind regimes with one, two, or three wind directions produce dunes with a unimodal orientation. There are two notable exceptions to this generalization. The first is where the wind modes are roughly orthogonal, which in some situations produce dunes with two orientations (Figs. 1.3, 1.9, 1.39, 1.45, 2.33; Fig. 5a and b). The second situation is where three radially symmetrical winds produce dunes with three orientations (Fig. 6a) or where three winds have imperfect symmetry and produce dunes with two orientations (Figs. 2.10, 2.20, 2.56; Fig. 6b and c). In other words, the number of crest orientations in a dune field is not a reliable indicator of the number of wind directions that formed the dunes, and the observed crests need not have been formed by winds perpendicular to them.

Tri-directional wind regimes over a starved bed form a wider range of dune morphologies than on a sand-covered bed. Increasing the divergence angle between the two strongest winds (moving from left to right across Figs. 3 and 4) produces a generalized sequence of: barchan dunes (the most unidirectional wind regime), squat barchans or domes, dunes with two or three crest orientations, to slug-shaped or boomerang-shaped dunes (reversing winds).

CRediT authorship contribution statement

David M. Rubin: Investigation, Methodology, Visualization, Writing – review & editing. **Olivier Rozier:** Data curation, Investigation, Methodology, Software, Visualization, Writing – review & editing. **Clément Narteau:** Investigation, Methodology, Resources, Software, Visualization, Writing – review & editing. **Sylvain Courrech du Pont:** Investigation, Methodology, Writing – review & editing.

Declaration of competing interest

The authors declare that they have no known competing financial interests or personal relationships that could have appeared to influence the work reported in this paper.

Data availability

We have provided a link to our data archive, which contains all the simulations and metadata used in this paper.

Acknowledgements

The authors acknowledge financial support from the NASA Mars Data Analysis Program, Grant 80NSSC19K1218; from the EOLE project of the French National Research Agency, ANR-23-CE56-0008; and from Initiative d'Excellence Université Paris Cité Grant ANR-18-IDEX-0001. Computing resources were provided by the NASA High-End Computing (HEC) Program through the NASA Advanced Supercomputing (NAS) Division at Ames Research Center. The authors thank Phillippe Claudin for discussions regarding λ_0.

References

Andreotti, B., Fourrière, A., Ould-Kaddour, F., Murray, B., Claudin, P., 2009. Giant aeolian dune size determined by the average depth of the atmospheric boundary layer. Nature 457, 1120.

Bagnold, R.A., 1941. The physics of blown sand and desert dunes. Methuen, London, p. 265.

Bourke, M.C., 2010. Barchan dune asymmetry: Observations from Mars and Earth. Icarus 205, 183–197. https://doi.org/10.1016/j.icarus.2009.08.023.
Chao, L., Zhibao, D., 2022. Distribution of dune landform on Mars: front. Astron. Space Sci. 9, 811702 https://doi.org/10.3389/fspas.2022.811702.
Claudin, P., Andreotti, B., 2006. A scaling law for aeolian dunes on Mars, venus, Earth, and for subaqueous ripples: Earth planet. Sci. Lett. 252, 30–44.
Courrech du Pont, S., Narteau, C., Gao, X., 2014. Two modes of dune formation. Geology 42, 743–746.
Durán Vinent, O., Andreotti, B., Claudin, P., Winter, C., 2019. A unified model of ripples and dunes in water and planetary environments. Nature Geoscience 12, 345–350. https://doi.org/10.1038/s41561-019-0336-.
Elbelrhiti, H., 2012. Initiation and early development of barchan dunes, a case study of the moroccan Atlantic Sahara Desert. Geomorphology 138, 181–188.
Elbelrhiti, H., Claudin, P., Andreotti, B., 2005. Field evidence for surface-wave induced instability of sand dunes. Nature 437, 04058.
Fernandez-Cascales, L., Lucas, A., Rodriguez, S., Gao, X., Spiga, A., Narteau, C., 2018. First quantification of relationship between dune orientation and sediment availability. Olympia Undae, Mars: Earth and Planetary Science Letters 489, 241–250.
Gadal C., Narteau, C., Courrech du Pont, S., Rozier, O., Claudin, P., 2020, Periodicity in fields of elongating dunes: Geology, 48:383-347.
Gadal, C., Narteau, C., Courrech du Pont, S., Rozier, O., Claudin, P., 2019. Incipient bedforms in a bidirectional wind regime. Journal of Fluid Mechanics 862, 490–516.
Gao, X., Narteau, C., Rozier, O., Courrech du Pont, 2015b, Phase diagrams of dune shape and orientation depending on sand availability: Scientific Reports, 5, doi:10.1038/srep14677.
Gao, X., Narteau, C., Rozier, O., 2015a. Development and steady states of transverse dunes: a numerical analysis of dune pattern coarsening and giant dunes. J. Geophys. Res. 120 (10), 2200–2219.
Gao, X., Gadal, C., Rozier, O., Narteau, C., 2018. Morphodynamics of barchan and dome dunes under variable wind regimes. Geology 46, 743–746.
Geissler, P.E., Wilgus, J.T., 2017. The morphology of transverse aeolian ridges on Mars. Aeolian Research 26, 63–71. https://doi.org/10.1016/j.aeolia.2016.08.008.
Gunn, A., 2023. Formation and reorganization time scales of aeolian landscapes. Geology 51, 351–355.
Hunter, R.E., Richmond, B.M., Alpha, T.R., 1983. Storm-controlled oblique dunes of the Oregon coast. Geological Society of America Bulletin 94, 1450–1465.
Kennedy, J.F., 1969. The formation of sediment ripples, dunes, and antidunes. Annual Review of Fluid Mechanics 1, 147–168.
Lapôtre, M.G.A., Ewing, R.C., Lamb, M.P., et al., 2016. Large wind ripples on Mars: A record of atmospheric evolution. Science 353, 55–58.
Lü, P., Dong, Z., & Rozier, O., 2018, The combined effect of sediment availability and wind regime on the morphology of aeolian sand dunes: Journal of Geophysical Research: Earth Surface, 1232878–2886. doi: 10.1029/2017jf004361.
Lü, P., Narteau, C., Dong, Z., Claudin, P., Rodriguez, S., An, Z., Gadal, C., Courrech du Pont, S., 2022, Coexistence of two dune growth mechanisms in a landscape-scale experiment: Geophysical Research Letters, 49, e2021GL097636.
Lü, P., Narteau, C., Dong, Z., Rozier, O., Courrech du Pont, S., 2017. Unravelling raked linear dunes to explain the coexistence of bedforms in complex dunefields: nat. Commun. 8, 14239. https://doi.org/10.1038/ncomms14239.
Lucas, A., Narteau, C., Rodriguez, S., Rozier, O., Callot, Y., Garcia, A., Courrech du Pont, S., 2015. Sediment flux from the morphodynamics of elongating linear dunes. Geology 43, 1027–1030.
Lv, P., Dong, Z., Narteau, C., Rozier, O., 2016. Morphodynamic mechanisms for the formation of asymmetric barchans: improvement of the bagnold and Tsoar models. Environ Earth Sci. 75, 259. https://doi.org/10.1007/s12665-015-5083-2.
Narteau, C., Zhang, D., Rozier, O., Claudin, P., 2009. Setting the length and time scales of a cellular automaton dune model from the analysis of superimposed bedforms. Journal of Geophysical Research 114, F03006.
Nishimori, H., and Tanaka, H., 2003, Simple model for the complex dynamics of dunes: In Concepts and Modelling in Geomorphology: International Perspectives (Evans, I. S.; Dikau, R.; Tokunaga, E.; Ohmori, H.; Hirano, M.; editors). TerraPub: 87-100. Tokyo.
Parteli, E.J.R., Durán, O., Tsoar, H., Schwämmle, V., Herrmann, H.J., 2009. Dune formation under bimodal winds: proc. Nat. Acad. Sci. 106, 22085–22089.
Parteli, E.J.R., Durán, Bourke, M.C., Tsoar, H., Pöschel, T., Herrmann, H., 2014. Origins of barchan dune asymmetry: insights from numerical simulations. Aeolian Research 12, 121–133.
Ping, L., Narteau, C., Dong, Z., Zhang, Z., Courrech du Pont, S., 2014. Emergence of oblique dunes in a landscape-scale experiment. Nat Geosci 7, 99–103.
Reffet, E., Courrech du Pont, S., Hersen, P., Douady, S., 2010. Formation and stability of transverse and longitudinal dunes. Geology 38, 491–494.
Rozier, O., Narteau, C., Rubin, D.M., Courrech du Pont, S., 2024. Simulations of dune morphology under tri-directional wind regimes. IPGP Research Collection. https://doi.org/10.18715/IPGP.2023.lqdzz72n.
Rozier, O., Narteau, C., 2014. A Real-Space Cellular Automaton Laboratory: Earth Surface Processes and Landforms 39, 98–109. https://doi.org/10.1002/esp.3479.
Rozier, O., Narteau, C., Gadal, C., Claudin, P., Courrech du Pont, S., 2019. Elongation and stability of a linear dune. Geophysical Research Letters 46, 14521–14530.
Rubin, D.M., 2012. A unifying model of planform straightness of ripples and dunes in air and water. Earth Science Reviews 113, 176–185.
Rubin, D.M, and McCulloch. 1980. Single and superimposed bedforms: A synthesis of San Francisco Bay and flume observations: *in* A.H. Bouma, D.S. Gorsline, G. Allen, and C. Monty, eds., *Shallow Marine Processes and Products*, Sedimentary Geology. 26. 207-231.
Rubin, D.M., Hesp, P.A., 2009. Multiple origins of linear dunes on Earth and titan. Nature Geoscience 2, 653–658.
Rubin, D.M., Hunter, R.E., 1987. Bedform Alignment in Directionally Varying Flow: Science 237, 276–278.
Rubin, D.M., Ikeda, H., 1990. Flume experiments on the alignment of transverse, oblique, and longitudinal dunes in directionally varying flows. Sedimentology 37, 673–684.
Schatz, V., Tsoar, H., Edgett, K.S., Parteli, E.J., Herrmann, H.J., 2006. Evidence for indurated sand dunes in the Martian north polar region. Journal of Geophysical Research: Planets 111 (E4).
Song, Q., Gao, X., Lei, J., Li, S., 2019. Spatial distribution of sand dunes and their relationship with fluvial systems on the southern margin of the Taklimakan Desert, China: geomatics. Natural Hazards and Risk 10 (1), 2408–2428. https://doi.org/10.1080/19475705.2019.1699607.
Stein, R.A., 1965. Laboratory studies of total load and apparent bed load: jour. Geophys. Res. 70, 1831–1842.
Tsoar, H., 1984. The formation of seif dunes from barchans—a discussion. Zeit. Für Geomorphology 28, 99–103.
Werner, B.T., 1995. Eolian dunes: computer simulations and attractor interpretation. Geology 23, 1107–1110.
Werner, B.T., Kocurek, G., 1997. Bedform dynamics: does the tail wag the dog? Geology 25, 771–774.
Zhang, D., Narteau, C., Rozier, O., et al., 2012. Morphology and Dynamics of Star Dunes from Numerical Modelling: Nature Geosci 5, 463–467. https://doi.org/10.1038/ngeo1503.
Zhang, D., Yang, X., Rozier, O., Narteau, C., 2014. Mean residence time in barchan dunes. J. Geophys. Res.: Earth Surf. 119, 451–463.
Zimbelman, J.R., 2010. Transverse aeolian ridges on Mars: first results from HiRISE images. Geomorphology 121, 22–29. https://doi.org/10.1016/j.geomorph.2009.05.012.